Publication III

Piippo, A., Hinkkanen, M., and Luomi, J. (2008). “Analysis of an adaptive observer for sensorless control of interior permanent magnet synchronous motors.” *IEEE Transactions on Industrial Electronics*, **55**(2), pp. 570-576.

Analysis of an Adaptive Observer for Sensorless Control of Interior Permanent Magnet Synchronous Motors

Antti Piippo, *Student Member, IEEE*, Marko Hinkkanen, *Member, IEEE*, and Jorma Luomi, *Member, IEEE*

***Abstract*—This paper deals with a speed and position estimation method for the sensorless control of permanent magnet synchronous motors. The method is based on a speed-adaptive observer. The dynamics of the system are analyzed by linearizing both the motor model and the observer, and the observer gain is selected to give improved damping and noise suppression. At low speeds, the observer is augmented with a signal injection technique, providing stable operation down to zero speed. The experimental results, obtained using a 2.2-kW interior magnet motor, are in agreement with the results of the analysis.**

***Index Terms*—Adaptive observers, motion control, permanent magnet motors, stability analysis.**

I. Introduction

THE INCREASING interest in permanent magnet synchronous machines (PMSMs) is due to their high torque-to-weight ratio and high efficiency. To control the PMSM, the rotor position and speed must be known. A position sensor is traditionally used, but the cost and the complexity of the drive system can be reduced by eliminating the sensor and its cabling. In sensorless control, the rotor position and speed are estimated from the measured electrical quantities by means of a fundamental-excitation method or a high-frequency (HF) signal-injection method. Fundamental-excitation methods are based on a mathematical model of the motor. They cannot be used for sustained operation at the lowest speeds since the back electromotive force (EMF) of the PMSM becomes very low. Signal-injection methods are based on detecting the anisotropy caused by the saliency of the rotor or by magnetic saturation. These methods are well suited to low speed operations, including zero speed. However, signal injection is usually not used at higher speeds since the additional voltage needed for signal injection becomes a restriction and HF currents cause unnecessary losses in the motor.

Various fundamental-excitation methods have been proposed for the estimation of the rotor position and speed. The stator flux and its position can be directly estimated from the motor terminal voltages and currents [1], and the load angle between the rotor and the stator flux can be compensated assuming steady state [2]. By using an adaptive (closed-loop) observer, the noise in the estimated angle can be reduced without degrading the dynamic performance. The adaptive observer consists of a state observer augmented with a speed adaptation loop. The state observer mimics the electrical dynamics of the PMSM. An observer gain can be used to modify the properties of the observer. An error term is calculated from the measured and estimated quantities, and the rotor speed is usually adjusted by a PI mechanism. The current or the stator flux has been used as a state variable of the observer [3]–[8]. An observer design using the stator flux error as a state variable has also been proposed [9]. The structure of the observer becomes more complicated if an extended EMF [10] is selected as a state variable. It is typical of interior magnet motors that the rotor saliency complicates the application and analysis of fundamental-excitation methods [2], [5], [7]–[10], contrary to signal injection methods.

The stability of the drive system is the most crucial design criterion [6], [8]. In this paper, an observer gain providing a stable and well damped system is proposed based on the linearized model of the system. The PMSM model and the adaptive observer are first defined. Then, the linearized model of the system is derived, and used for analyzing different gains. The method for coupling the signal injection to the adaptive observer [7] at low speeds is summarized. Finally, experimental results are presented.

II. PMSM Model

The PMSM is modeled in the $d-q$ reference frame fixed to the rotor. The d-axis is oriented along the permanent magnet flux, whose angle in the stator reference frame is θ_m in electrical radians. The stator voltage equation is

$$\mathbf{u}_\mathrm{s} = R_\mathrm{s}\mathbf{i}_\mathrm{s} + \dot{\boldsymbol{\psi}}_\mathrm{s} + \omega_\mathrm{m}\mathbf{J}\boldsymbol{\psi}_\mathrm{s} \tag{1}$$

where $\mathbf{u}_\mathrm{s} = [\,u_d \quad u_q\,]^\mathrm{T}$ is the stator voltage, $\mathbf{i}_\mathrm{s} = [\,i_d \quad i_q\,]^\mathrm{T}$ the stator current, $\boldsymbol{\psi}_\mathrm{s} = [\,\psi_d \quad \psi_q\,]^\mathrm{T}$ the stator flux, R_s the stator resistance, $\omega_\mathrm{m} = \dot{\theta}_\mathrm{m}$ the electrical angular speed of the rotor, and

$$\mathbf{J} = \begin{bmatrix} 0 & -1 \\ 1 & 0 \end{bmatrix}.$$

The stator flux is

$$\boldsymbol{\psi}_\mathrm{s} = \mathbf{L}\mathbf{i}_\mathrm{s} + \boldsymbol{\psi}_\mathrm{pm} \tag{2}$$

Manuscript received March 31, 2006; revised October 22, 2007. This work was supported by ABB Oy and Walter Ahlström Foundation.

The authors are with the Power Electronics Laboratory, Department of Electrical and Communications Engineering, Helsinki University of Technology, 02015 Espoo, Finland (e-mail: antti.piippo@tkk.fi).

Digital Object Identifier 10.1109/TIE.2007.911949

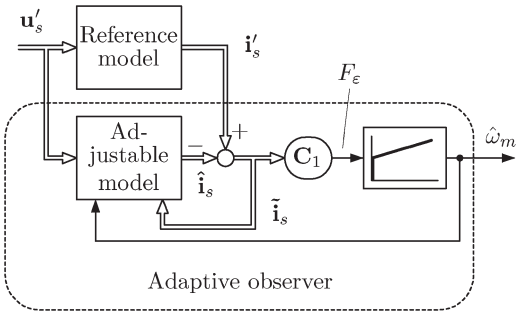

Fig. 1. Block diagram of the adaptive observer. In addition, the reference model (the actual motor) is shown.

where $\boldsymbol{\psi}_{\mathrm{pm}} = [\,\psi_{\mathrm{pm}} \quad 0\,]^{\mathrm{T}}$ is the permanent magnet flux and

$$\mathbf{L} = \begin{bmatrix} L_d & 0 \\ 0 & L_q \end{bmatrix}$$

is the inductance matrix, L_d and L_q being the direct- and quadrature-axis inductances, respectively. The electromagnetic torque is given by

$$T_e = \frac{3p}{2}\psi_{\mathrm{s}}^{\mathrm{T}}\mathbf{J}^{\mathrm{T}}\mathbf{i}_{\mathrm{s}} \tag{3}$$

where p is the number of pole pairs.

III. Adaptive Observer

In an adaptive observer, the rotor speed and position estimation is based on the estimation error between two different models; the actual motor can be considered as a reference model and the observer—including the rotor speed estimate $\hat{\omega}_{\mathrm{m}}$—as an adjustable model [3]. An error term used in an adaptation mechanism is constructed from the estimation error of the stator current. The output of the adaptation mechanism, usually the rotor speed, is fed back to the adjustable model.

In the following, the adaptive observer is formulated in the estimated rotor reference frame. The block diagram of the adaptive observer is shown in Fig. 1. The stator flux is selected as a state variable in the adjustable model. The model is based on (1) and (2), and defined by

$$\dot{\hat{\boldsymbol{\psi}}}_{\mathrm{s}} = \mathbf{u}'_{\mathrm{s}} - \hat{R}_{\mathrm{s}}\hat{\mathbf{i}}_{\mathrm{s}} - \hat{\omega}_{\mathrm{m}}\mathbf{J}\hat{\boldsymbol{\psi}}_{\mathrm{s}} + \boldsymbol{\lambda}\tilde{\mathbf{i}}_{\mathrm{s}} \tag{4}$$

where estimated quantities are marked by $\hat{}$ and measured quantities expressed in the estimated rotor reference frame are marked by $'$. The estimate of the stator current and the estimation error of the stator current are

$$\hat{\mathbf{i}}_{\mathrm{s}} = \hat{\mathbf{L}}^{-1}(\hat{\boldsymbol{\psi}}_{\mathrm{s}} - \hat{\boldsymbol{\psi}}_{\mathrm{pm}}) \tag{5}$$

and

$$\tilde{\mathbf{i}}_{\mathrm{s}} = \mathbf{i}'_{\mathrm{s}} - \hat{\mathbf{i}}_{\mathrm{s}}, \tag{6}$$

respectively. The observer gain is

$$\boldsymbol{\lambda} = \lambda_1\mathbf{I} + \lambda_2\mathbf{J} \tag{7}$$

where $\mathbf{I}$ is the two-by-two identity matrix, and λ_1 and λ_2 are scalar gain parameters. A pure voltage model is obtained by selecting $\lambda_1 = -\hat{R}_{\mathrm{s}}$ and $\lambda_2 = 0$, leading to the sole use of the measured current in (4) instead of the estimated current. If $\lambda_1 = 0$ and $\lambda_2 = 0$ are chosen, the measured current affects (4) only through the speed estimate $\hat{\omega}_{\mathrm{m}}$.

There are various alternatives for obtaining an error term from the current error. In the following, the error term is defined:

$$F_\varepsilon = \mathbf{C}_1\tilde{\mathbf{i}}_{\mathrm{s}} \tag{8}$$

where $\mathbf{C}_1 = [\,0 \quad \hat{L}_q\,]$. Hence, the current error in the estimated q-direction is used for adaptation. The estimate of the electrical angular speed of the rotor is obtained by a PI speed adaptation mechanism

$$\hat{\omega}_{\mathrm{m}} = -k_{\mathrm{p}}F_\varepsilon - k_{\mathrm{i}}\int F_\varepsilon\, dt \tag{9}$$

where k_{p} and k_{i} are nonnegative gains. The estimate $\hat{\theta}_{\mathrm{m}}$ for the rotor position is obtained by integrating $\hat{\omega}_{\mathrm{m}}$.

The gains k_{p} and k_{i} of the adaptation mechanism are selected by omitting the electrical dynamics of the system, resulting in [7]

$$k_{\mathrm{p}} = \frac{2\alpha_{\mathrm{fo}}}{\hat{\psi}_{\mathrm{pm}}}, \quad k_{\mathrm{i}} = \frac{\alpha_{\mathrm{fo}}^2}{\hat{\psi}_{\mathrm{pm}}} \tag{10}$$

where the design parameter α_{fo} corresponds to the approximate bandwidth of the adaptive observer.

IV. Dynamic Analysis

A. Linearization

In the following, the focus is on the dynamic properties of the adaptive observer. The dynamics of the current estimation error are derived, and combined with the speed adaptation mechanism for investigating the stability and damping of the adaptive observer. It is assumed that the estimates of the motor parameters are exact.

The dynamics of the current estimation error (6) are first linearized. For this purpose, both the dynamics of the motor current and the dynamics of the adaptive observer are considered. The result is

$$\begin{aligned}\dot{\tilde{\mathbf{i}}}_{\mathrm{s}} = {} & \underbrace{\left(-R_{\mathrm{s}}\mathbf{L}^{-1} - \omega_{\mathrm{m0}}\mathbf{L}^{-1}\mathbf{J}\mathbf{L} - \mathbf{L}^{-1}\boldsymbol{\lambda}\right)}_{\mathbf{A}_1}\tilde{\mathbf{i}}_{\mathrm{s}} \\ & + \underbrace{\left(\mathbf{J}\mathbf{i}_{\mathrm{s0}} - \mathbf{L}^{-1}\mathbf{J}\mathbf{L}\mathbf{i}_{\mathrm{s0}} - \mathbf{L}^{-1}\mathbf{J}\boldsymbol{\psi}_{\mathrm{pm}}\right)}_{\mathbf{B}_1}\tilde{\omega}_{\mathrm{m}} \\ & + \underbrace{\left(\omega_{\mathrm{m0}}\mathbf{L}^{-1}\mathbf{J}\mathbf{L}\mathbf{J}\mathbf{i}_{\mathrm{s0}} + \omega_{\mathrm{m0}}\mathbf{i}_{\mathrm{s0}} + \omega_{\mathrm{m0}}\mathbf{L}^{-1}\boldsymbol{\psi}_{\mathrm{pm}}\right)}_{\mathbf{A}_2}\tilde{\theta}_{\mathrm{m}}\end{aligned} \tag{11}$$

where operating-point quantities are marked by the subscript 0, $\tilde{\omega}_{\mathrm{m}} = \omega_{\mathrm{m}} - \hat{\omega}_{\mathrm{m}}$ is the speed estimation error, and $\tilde{\theta}_{\mathrm{m}} = \theta_{\mathrm{m}} - \hat{\theta}_{\mathrm{m}}$ the position estimation error. The derivation of (11) is presented in the Appendix. To formulate a single-input

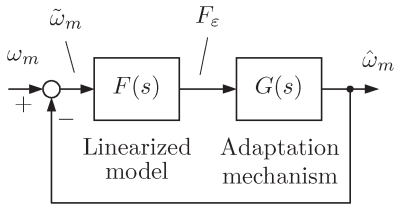

Fig. 2. Block diagram of the linearized model of the adaptive observer.

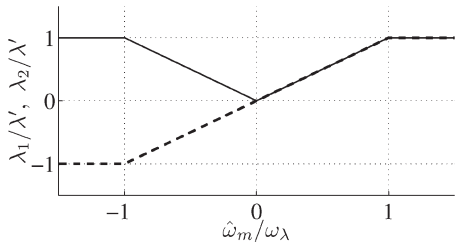

Fig. 3. Observer gain parameters λ_1 (solid) and λ_2 (dashed) as a function of the estimated rotor speed.

single-output system, the rotor position error $\tilde{\theta}_\mathrm{m}$ is chosen as a state variable in addition to the current error, and (8) is also used. The resulting state-space representation can be written as

$$\begin{bmatrix} \dot{\tilde{\mathbf{i}}}_\mathrm{s} \\ \dot{\tilde{\theta}}_\mathrm{m} \end{bmatrix} = \underbrace{\begin{bmatrix} \mathbf{A}_1 & \mathbf{A}_2 \\ \mathbf{0} & 0 \end{bmatrix}}_{\mathbf{A}} \begin{bmatrix} \tilde{\mathbf{i}}_\mathrm{s} \\ \tilde{\theta}_\mathrm{m} \end{bmatrix} + \underbrace{\begin{bmatrix} \mathbf{B}_1 \\ 1 \end{bmatrix}}_{\mathbf{B}} \tilde{\omega}_\mathrm{m}$$

$$F_\varepsilon = \underbrace{[\,\mathbf{C}_1 \quad 0\,]}_{\mathbf{C}} \begin{bmatrix} \tilde{\mathbf{i}}_\mathrm{s} \\ \tilde{\theta}_\mathrm{m} \end{bmatrix}. \tag{12}$$

Hence, the transfer function from the speed error $\tilde{\omega}_\mathrm{m}(s)$ to the error term $F_\varepsilon(s)$ is given by

$$F(s) = \mathbf{C}(s\mathbf{I} - \mathbf{A})^{-1}\mathbf{B}. \tag{13}$$

According to the adaptation mechanism (9), the transfer function from the error term $F_\varepsilon(s)$ to the speed estimate $\hat{\omega}_\mathrm{m}(s)$ is

$$G(s) = -k_\mathrm{p} - \frac{k_\mathrm{i}}{s}. \tag{14}$$

Using (13) and (14), the closed-loop system shown in Fig. 2 is obtained. The resulting closed-loop transfer function

$$G_\mathrm{c}(s) = \frac{F(s)G(s)}{1 + F(s)G(s)} \tag{15}$$

from $\omega_\mathrm{m}(s)$ to $\hat{\omega}_\mathrm{m}(s)$ can be evaluated for any operating point.

B. Observer Gain Selection

The observer gain $\boldsymbol{\lambda} = \lambda_1\mathbf{I} + \lambda_2\mathbf{J}$ can be selected in different ways. Using the pole placement design for gain selection is rather complicated due to the fourth-order closed-loop transfer function. A simple alternative is to use zero gain, or to select a constant gain $\lambda_1 > -\hat{R}_\mathrm{s}$ and $\lambda_2 = 0$. A negative constant gain was used for PMSM drives in [7]. Better damping can be achieved by selecting a speed-dependent gain

$$\lambda_1 = \begin{cases} \lambda' \frac{|\hat{\omega}_\mathrm{m}|}{\omega_\lambda}, & |\hat{\omega}_\mathrm{m}| \le \omega_\lambda \\ \lambda', & |\hat{\omega}_\mathrm{m}| > \omega_\lambda \end{cases} \tag{16a}$$

$$\lambda_2 = \begin{cases} \lambda' \frac{\hat{\omega}_\mathrm{m}}{\omega_\lambda}, & |\hat{\omega}_\mathrm{m}| \le \omega_\lambda \\ \lambda' \mathrm{sign}(\hat{\omega}_\mathrm{m}), & |\hat{\omega}_\mathrm{m}| > \omega_\lambda \end{cases} \tag{16b}$$

which is similar to the gain used in an adaptive full-order flux observer for induction motor drives [11]. The gain parameters are illustrated in Fig. 3. The positive constants λ' and ω_λ can be selected based on the linearized model.

The poles of the closed-loop transfer function $G_\mathrm{c}(s)$ were evaluated by using the Control System Toolbox of the MATLAB software. The data given in Section VI were used for the motor and for the speed adaptation, and the operating-point stator current $\mathbf{i}_{\mathrm{s}0}$ was defined according to maximum torque per current control [12]. Fig. 4 shows the variation of the poles of $G_\mathrm{c}(s)$ for positive nominal torque and varying speed (-1 p.u. $\le \omega_{\mathrm{m}0} \le 1$ p.u.). The motor works in the motoring mode at positive speeds and in the regenerating mode at negative speeds.

In Fig. 4, the observer gains are: (a) zero gain; (b) constant gain $\lambda_1 = -0.5\hat{R}_\mathrm{s}$ and $\lambda_2 = 0$; (c) speed-dependent gain (16) with $\lambda' = 2\hat{R}_\mathrm{s}$ and $\omega_\lambda = 1$ p.u. With the exception of very low speeds, the poles are located in the left half of the complex plane and the linearized system is stable. In the case of the zero gain in Fig. 4(a), one of the upper-half-plane poles shown remains near the imaginary axis but moves far away from the real axis as the speed increases. This pole location indicates poor damping at high speeds. In the case of the constant gain in Fig. 4(b), the corresponding pole is closer to the imaginary axis. The damping is thus even worse than that obtained with zero gain. Because the speed-dependent gain is used in Fig. 4(c), the poles move away from the imaginary axis as the speed increases. The damping at high speeds is thus improved.

It is worth noticing that different pole locations are obtained at equal speeds in the motoring and regenerating modes of operation. These differences originate from the rotor saliency; the dependence on the load condition disappears if $L_d = L_q$.

At very low speeds (approximately $|\omega_{\mathrm{m}0}| < 0.02$ p.u.) in the motoring mode, one of the poles moves to the right half-plane along the real axis for all the observer gains investigated. This phenomenon can be seen in Fig. 5, where the vicinity of the origin of Fig. 4(c) is magnified. The low-speed instability originates from the rotor saliency; the linearized system is stable (marginally stable at zero speed) in the whole operating region if $L_d = L_q$. A similar unstable region has been found at low speeds in [13], where a different observer was used.

Simulation results in Fig. 6 illustrate the operation at very low speeds. Accurate motor parameter estimates and the speed-dependent observer gain (16) are used. The positive nominal load torque is applied stepwise at $t = 1$ s in Fig. 6(a) and (b) corresponding to the motoring mode, while the negative load is applied in Fig. 6(c) corresponding to the regenerating mode. The speed reference is 0.01 p.u. in Fig. 6(a) and (c), and 0.03 p.u. in Fig. 6(b). As predicted by the linearized model, the system becomes unstable in the case of Fig. 6(a) while the system remains stable in Fig. 6(b) and (c).

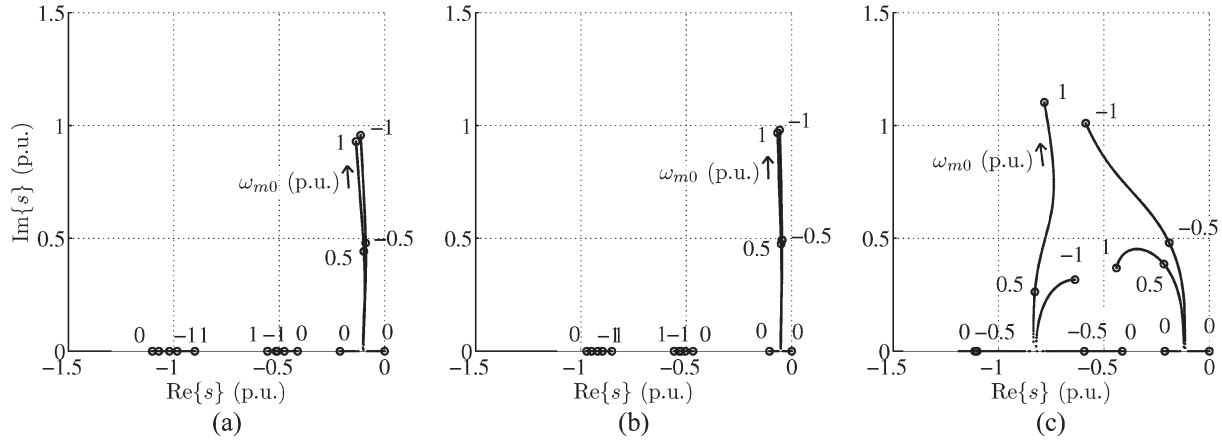

Fig. 4. Variation of poles of $G_{\rm c}(s)$ at nominal load as rotor speed $\omega_{\rm m0}$ is varied: (a) zero observer gain; (b) constant gain; and (c) speed-dependent gain. Because of symmetry, only the upper half-plane is shown.

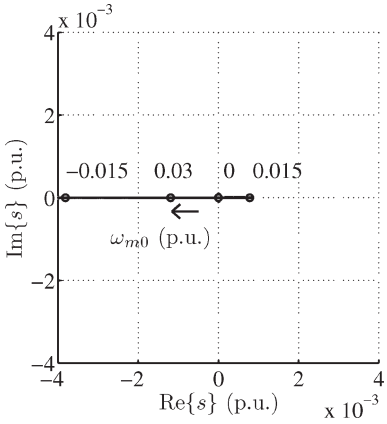

Fig. 5. Magnification of Fig. 4(c).

V. Coupling HF Signal Injection to the Adaptive Observer

The low-speed operation can be stabilized by augmenting the adaptive observer with an HF signal injection method at low speeds. Furthermore, the signal injection method makes the system robust against errors in measurements and motor parameters. The method for coupling the signal injection to the adaptive observer has been presented in [7], and is summarized here.

An alternating voltage was selected for HF signal injection. A carrier excitation signal varying sinusoidally at angular frequency $\omega_{\rm c}$ and having amplitude $\hat{u}_{\rm c}$, i.e.,

$$u_{\rm c} = \hat{u}_{\rm c}\cos(\omega_{\rm c} t) \tag{17}$$

is superimposed on the d component of the stator voltage in the estimated rotor reference frame. An alternating HF current response is detected in the q-direction of the estimated rotor reference frame, amplitude modulated by the rotor position estimation error. The q component of the measured current is band-pass filtered (BPF), giving an HF current signal $i_{\rm qc}$ that varies at the signal injection frequency. The current signal is then demodulated and low-pass filtered (LPF) to extract an error signal

$$\varepsilon = {\rm LPF}\left\{i_{\rm qc}\sin(\omega_{\rm c} t)\right\}. \tag{18}$$

Ideally, this error signal is

$$\varepsilon = \underbrace{\frac{\hat{u}_{\rm c}}{\omega_{\rm c}}\frac{L_q - L_d}{4L_q L_d}}_{K_\varepsilon}\sin(2\tilde{\theta}_{\rm m}) \tag{19}$$

where K_ε is the signal injection gain and $\tilde{\theta}_{\rm m} = \theta_{\rm m} - \hat{\theta}_{\rm m}$ is the estimation error of the rotor position.

The error signal is used for correcting the estimated position by influencing the direction of the stator flux estimate of the adjustable model (4). The algorithm is given by

$$\dot{\hat{\boldsymbol{\psi}}}_{\rm s} = \mathbf{u}'_{\rm s} - \hat{R}_{\rm s}\hat{\mathbf{i}}_{\rm s} - (\hat{\omega}_{\rm m} - \omega_\varepsilon)\mathbf{J}\hat{\boldsymbol{\psi}}_{\rm s} + \boldsymbol{\lambda}\tilde{\mathbf{i}}_{\rm s} \tag{20}$$

$$\omega_\varepsilon = \gamma_{\rm p}\varepsilon + \gamma_{\rm i}\int \varepsilon\, dt \tag{21}$$

where $\gamma_{\rm p}$ and $\gamma_{\rm i}$ are the gains of the PI mechanism driving the error signal ε to zero. In accordance with [14], these gains are selected as

$$\gamma_{\rm p} = \frac{\alpha_{\rm i}}{2K_\varepsilon}, \quad \gamma_{\rm i} = \frac{\alpha_{\rm i}^2}{6K_\varepsilon} \tag{22}$$

where $\alpha_{\rm i}$ is the approximate bandwidth of the PI mechanism. At low speeds, the combined observer relies both on the signal injection method and on the adaptive observer. The influence of the HF signal injection is decreased linearly with increasing speed by decreasing both $\hat{u}_{\rm c}$ and $\alpha_{\rm i}$, reaching zero at transition speed ω_Δ. At speeds above ω_Δ, the estimation is based only on the adaptive observer. The integral in (21) settles to a value that compensates the effect of parameter and measurement errors. To improve the operation at transients, the integral should be bounded by reasonable limits.

VI. Experimental Results

The different observer gains were investigated by means of simulations and laboratory experiments. The block diagram of the control system comprising cascaded speed and current control loops is shown in Fig. 7. IP-type speed control is used, and the current control is implemented as PI-type control in the estimated rotor reference frame. The current component

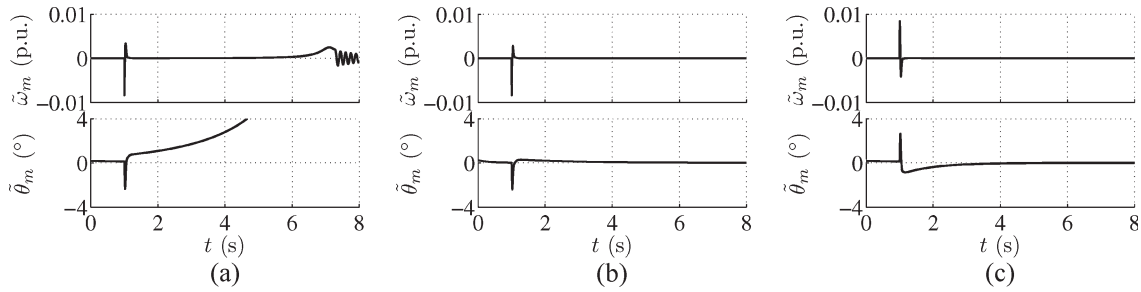

Fig. 6. Simulation results showing low-speed operation at nominal load torque: (a) $\omega_{\rm m} = 0.01$ p.u., motoring mode; (b) $\omega_{\rm m} = 0.03$ p.u., motoring mode; and (c) $\omega_{\rm m} = 0.01$ p.u., regenerating mode. The first subplot shows speed estimation error, while the second subplot shows position estimation error.

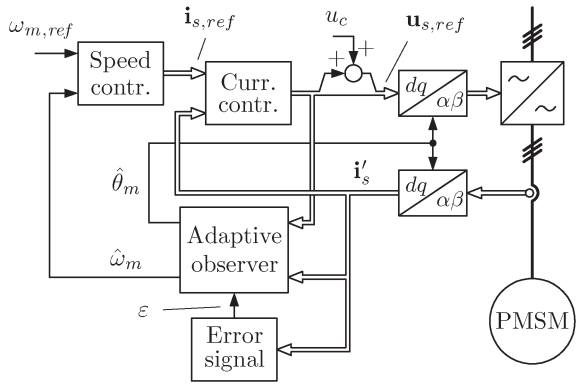

Fig. 7. Block diagram of the control system. Block "Speed contr." includes both the speed controller and the calculation of the current references. Block "Adaptive observer" includes the observer combined with signal injection according to (20) and (21).

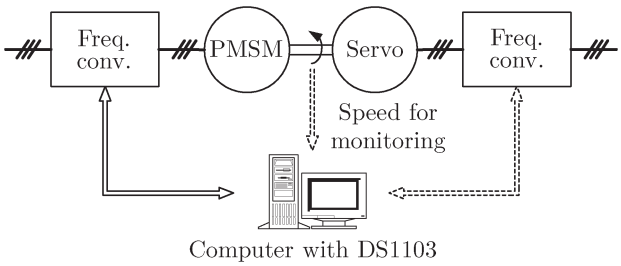

Fig. 8. Experimental setup. Mechanical load is provided by a servodrive.

references $i_{d,\rm ref}$ and $i_{q,\rm ref}$ are calculated according to maximum torque per current control [12]. The dc-link voltage of the converter is measured, and a simple current feedforward compensation for dead times and power device voltage drops is applied [15].

The experimental setup is illustrated in Fig. 8. A six-pole interior-magnet PMSM (2.2 kW, 1500 r/min) is fed by a frequency converter that is controlled by a dSPACE DS1103 PPC/DSP board. The motor data are given in Table I. Mechanical load is provided by a PMSM servodrive. An incremental encoder is used for monitoring the actual rotor speed and position. The nominal dc-link voltage is 540 V, and the switching frequency and the sampling frequency are both 5 kHz. The HF carrier excitation signal has a frequency of 833 Hz and an amplitude of 40 V, and the transition speed $\omega_\Delta = 0.13$ p.u. The electromagnetic torque is limited to 22 N · m, which is 1.57 times the nominal torque $T_{\rm N}$. Other parameters of the control system are given in Table II. The motor has harmonics in the

TABLE I
MOTOR DATA

Nominal power	2.2 kW
Nominal voltage	370 V
Nominal current	4.3 A
Nominal frequency	75 Hz
Nominal speed	1 500 r/min
Nominal torque T_N	14.0 Nm
Number of pole pairs p	3
Stator resistance R_s	3.59 Ω
Direct-axis inductance L_d	0.036 H
Quadrature-axis inductance L_q	0.051 H
Permanent magnet flux ψ_{pm}	0.545 Vs
Total moment of inertia	0.015 kgm^2

TABLE II
CONTROL SYSTEM PARAMETERS

Current controller bandwidth	2π·400 rad/s
Speed controller bandwidth	2π·5 rad/s
Speed adaptation bandwidth α_{fo}	2π·50 rad/s
Bandwidth α_i at zero speed	2π·5 rad/s

permanent magnet flux and stator inductances, causing some sixth-harmonic ripple in the torque and estimated position.

Fig. 9 shows experimental results obtained at the nominal load torque. The speed reference was first changed stepwise from zero to 0.67 p.u. at $t = 1$ s, then reversed to -0.67 p.u. at $t = 2$ s, and finally set to zero at $t = 3$ s. The constant gain $\lambda_1 = -0.5\hat{R}_{\rm s}$ and $\lambda_2 = 0$ was used in Fig. 9(a), and the speed-dependent gain (16) with $\lambda' = 2\hat{R}_{\rm s}$ and $\omega_\lambda = 1$ p.u. was used in Fig. 9(b). In both cases, the estimated rotor speed follows the actual speed closely during fast changes in the electromagnetic torque. It can be seen that the speed-dependent gain damps the vibrations more effectively than the constant gain. Moreover, the estimation error of the rotor position remains slightly smaller when using the speed-dependent gain. A comparison with the results obtained using a voltage model [14] reveals a significant improvement in the performance. This comparison is relevant since the same experimental setup was used in [14]. Persistent operation at zero speed under nominal load is possible due to the HF signal injection, which is in use at low speeds.

Fig. 10 shows experimental results from a slow speed reversal in the case of the speed-dependent gain. The load torque was kept at the nominal value between $t = 2$ s and $t = 28$ s, and the speed reference was changed from 0.67 p.u. to -0.67 p.u. between $t = 4$ s and $t = 26$ s. The estimated rotor speed follows the actual speed smoothly in the whole speed range in both motoring and regenerating modes. The noise

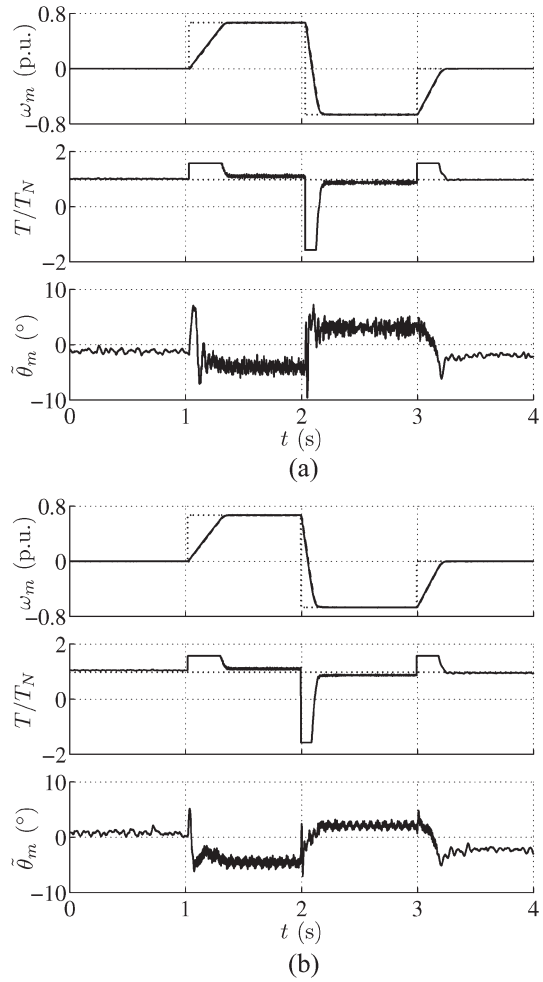

Fig. 9. Experimental results showing speed reference steps at nominal load torque: (a) constant gain and (b) speed-dependent gain. The first subplot shows electrical angular speed (solid), its estimate (dashed), and its reference (dotted). The second subplot shows estimated electromagnetic torque (solid) and load torque reference (dotted). The last subplot shows estimation error of rotor position in electrical degrees.

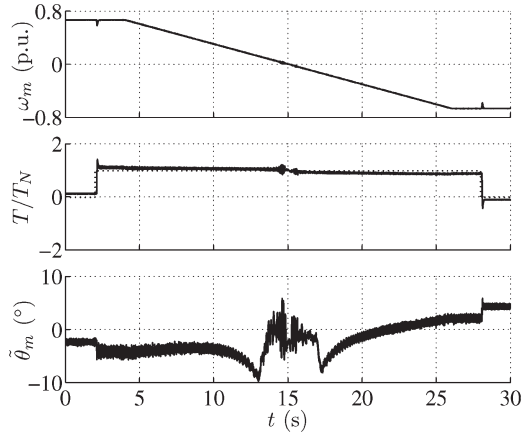

Fig. 10. Experimental results showing slow speed reversal at nominal load torque with speed-dependent gain. Explanations of the curves are as in Fig. 9.

is rejected effectively, and the estimation error of the rotor position is small even when a nominal load torque step is applied. The effect of the HF signal injection can be seen at low speeds; the estimation error of the rotor position increases with decreasing speed, but decreases rapidly when signal injection is used at $\hat{\omega}_{\mathrm{m}} = 0.13$ p.u. The ripple appearing at low speeds is related to the HF signal injection method, which is sensitive to stator inductance harmonics and errors in measured phase currents.

VII. Conclusion

The dynamic properties of the adaptive observer with different observer gains and in varying operating conditions can be investigated using a linearized model derived for the motor and observer. According to the analysis, damping at high speeds can be improved by selecting a speed-dependent observer gain. The experimental results are in agreement with the results of the analysis. The rotor speed and position can be estimated in a wide speed range, including zero speed, by means of an adaptive observer that is augmented with an HF signal injection technique at low speeds. The proposed speed-dependent observer gain improves the capability of damping unwanted vibrations and noise.

Appendix
Current Error Linearization

The stator current derivative based on (1) and (2) is

$$\dot{\mathbf{i}}_{\mathrm{s}} = \mathbf{L}^{-1}\mathbf{u}_{\mathrm{s}} - R_{\mathrm{s}}\mathbf{L}^{-1}\mathbf{i}_{\mathrm{s}} - \omega_{\mathrm{m}}\mathbf{L}^{-1}\mathbf{J}\mathbf{L}\mathbf{i}_{\mathrm{s}} - \omega_{\mathrm{m}}\mathbf{L}^{-1}\mathbf{J}\boldsymbol{\psi}_{\mathrm{pm}}. \tag{23}$$

The stator current transformed from the true rotor reference frame to the estimated rotor reference frame is

$$\mathbf{i}'_{\mathrm{s}} = \mathbf{T}\mathbf{i}_{\mathrm{s}} \tag{24}$$

where $\mathbf{T} = \cos\tilde{\theta}_{\mathrm{m}}\mathbf{I} + \sin\tilde{\theta}_{\mathrm{m}}\mathbf{J}$ is a coordinate transformation matrix, $\tilde{\theta}_{\mathrm{m}} = \theta_{\mathrm{m}} - \hat{\theta}_{\mathrm{m}}$ being the rotor position error. Combining (23) and (24) gives the current dynamics in the estimated rotor reference frame

$$\begin{aligned}\dot{\mathbf{i}}'_{\mathrm{s}} = {} & \tilde{\omega}_{\mathrm{m}}\mathbf{J}\mathbf{i}'_{\mathrm{s}} - R_{\mathrm{s}}\mathbf{T}\mathbf{L}^{-1}\mathbf{T}^{-1}\mathbf{i}'_{\mathrm{s}} - \omega_{\mathrm{m}}\mathbf{T}\mathbf{L}^{-1}\mathbf{J}\mathbf{L}\mathbf{T}^{-1}\mathbf{i}'_{\mathrm{s}} \\ & - \omega_{\mathrm{m}}\mathbf{T}\mathbf{L}^{-1}\mathbf{J}\boldsymbol{\psi}_{\mathrm{pm}} + \mathbf{T}\mathbf{L}^{-1}\mathbf{T}^{-1}\mathbf{u}'_{\mathrm{s}}\end{aligned} \tag{25}$$

where $\tilde{\omega}_{\mathrm{m}} = \omega_{\mathrm{m}} - \hat{\omega}_{\mathrm{m}}$ is the rotor speed error and $\mathbf{u}'_{\mathrm{s}} = \mathbf{T}\mathbf{u}_{\mathrm{s}}$. Linearizing this equation results in

$$\begin{aligned}\dot{\mathbf{i}}'_{\mathrm{s}} = {} & \left(-R_{\mathrm{s}}\mathbf{L}^{-1} - \omega_{\mathrm{m0}}\mathbf{L}^{-1}\mathbf{J}\mathbf{L}\right)\mathbf{i}'_{\mathrm{s}} \\ & + \mathbf{J}\mathbf{i}_{\mathrm{s0}}\tilde{\omega}_{\mathrm{m}} + \left(-\mathbf{L}^{-1}\mathbf{J}\mathbf{L}\mathbf{i}_{\mathrm{s0}} - \mathbf{L}^{-1}\mathbf{J}\boldsymbol{\psi}_{\mathrm{pm}}\right)\omega_{\mathrm{m}} \\ & + \big(R_{\mathrm{s}}\mathbf{L}^{-1}\mathbf{J}\mathbf{i}_{\mathrm{s0}} - R_{\mathrm{s}}\mathbf{J}\mathbf{L}^{-1}\mathbf{i}_{\mathrm{s0}} + \omega_{\mathrm{m0}}\mathbf{L}^{-1}\mathbf{J}\mathbf{L}\mathbf{J}\mathbf{i}_{\mathrm{s0}} \\ & - \omega_{\mathrm{m0}}\mathbf{J}\mathbf{L}^{-1}\mathbf{J}\mathbf{L}\mathbf{i}_{\mathrm{s0}} - \omega_{\mathrm{m0}}\mathbf{J}\mathbf{L}^{-1}\mathbf{J}\boldsymbol{\psi}_{\mathrm{pm}} \\ & - \mathbf{L}^{-1}\mathbf{J}\mathbf{u}_{\mathrm{s0}} + \mathbf{J}\mathbf{L}^{-1}\mathbf{u}_{\mathrm{s0}}\big)\tilde{\theta}_{\mathrm{m}} + \mathbf{L}^{-1}\mathbf{u}'_{\mathrm{s}}.\end{aligned} \tag{26}$$

The adjustable model (4) of the observer is rewritten in terms of the estimated current (5)

$$\begin{aligned}\dot{\hat{\mathbf{i}}}_{\mathrm{s}} = {} & -R_{\mathrm{s}}\mathbf{L}^{-1}\hat{\mathbf{i}}_{\mathrm{s}} - \hat{\omega}_{\mathrm{m}}\mathbf{L}^{-1}\mathbf{J}\mathbf{L}\hat{\mathbf{i}}_{\mathrm{s}} \\ & - \hat{\omega}_{\mathrm{m}}\mathbf{L}^{-1}\mathbf{J}\boldsymbol{\psi}_{\mathrm{pm}} + \mathbf{L}^{-1}\mathbf{u}'_{\mathrm{s}} + \mathbf{L}^{-1}\boldsymbol{\lambda}\tilde{\mathbf{i}}_{\mathrm{s}}.\end{aligned} \tag{27}$$

Linearizing and simplifying yields

$$\dot{\tilde{\mathbf{i}}}_{\mathrm{s}} = (-R_{\mathrm{s}}\mathbf{L}^{-1} - \omega_{\mathrm{m0}}\mathbf{L}^{-1}\mathbf{J}\mathbf{L} - \mathbf{L}^{-1}\boldsymbol{\lambda})\hat{\mathbf{i}}_{\mathrm{s}} + (-\mathbf{L}^{-1}\mathbf{J}\mathbf{L}\mathbf{i}_{\mathrm{s0}} - \mathbf{L}^{-1}\mathbf{J}\boldsymbol{\psi}_{\mathrm{pm}})\hat{\omega}_{\mathrm{m}} + \mathbf{L}^{-1}\boldsymbol{\lambda}\mathbf{i}'_{\mathrm{s}} + \mathbf{L}^{-1}\mathbf{u}'_{\mathrm{s}}. \quad (28)$$

Finally, the linearized equation of the current error $\tilde{\mathbf{i}}_{\mathrm{s}} = \mathbf{i}'_{\mathrm{s}} - \hat{\mathbf{i}}_{\mathrm{s}}$ is obtained by subtracting (28) from (26) and substituting

$$\mathbf{u}_{\mathrm{s0}} = R_{\mathrm{s}}\mathbf{i}_{\mathrm{s0}} + \omega_{\mathrm{m0}}\mathbf{J}\mathbf{L}\mathbf{i}_{\mathrm{s0}} + \omega_{\mathrm{m0}}\mathbf{J}\boldsymbol{\psi}_{\mathrm{pm}} \quad (29)$$

for the operating-point voltage. The result is

$$\dot{\tilde{\mathbf{i}}}_{\mathrm{s}} = (-R_{\mathrm{s}}\mathbf{L}^{-1} - \omega_{\mathrm{m0}}\mathbf{L}^{-1}\mathbf{J}\mathbf{L} - \mathbf{L}^{-1}\boldsymbol{\lambda})\tilde{\mathbf{i}}_{\mathrm{s}} + (\mathbf{J}\mathbf{i}_{\mathrm{s0}} - \mathbf{L}^{-1}\mathbf{J}\mathbf{L}\mathbf{i}_{\mathrm{s0}} - \mathbf{L}^{-1}\mathbf{J}\boldsymbol{\psi}_{\mathrm{pm}})\tilde{\omega}_{\mathrm{m}} + (\omega_{\mathrm{m0}}\mathbf{L}^{-1}\mathbf{J}\mathbf{L}\mathbf{J}\mathbf{i}_{\mathrm{s0}} + \omega_{\mathrm{m0}}\mathbf{i}_{\mathrm{s0}} + \omega_{\mathrm{m0}}\mathbf{L}^{-1}\boldsymbol{\psi}_{\mathrm{pm}})\tilde{\theta}_{\mathrm{m}}. \quad (30)$$

ACKNOWLEDGMENT

The authors would like to thank the reviewers for their professional work and helpful suggestions.

REFERENCES

[1] R. Wu and G. R. Slemon, "A permanent magnet motor drive without a shaft sensor," *IEEE Trans. Ind. Appl.*, vol. 27, no. 5, pp. 1005–1011, Sep./Oct. 1991.

[2] A. Consoli, S. Musumeci, A. Raciti, and A. Testa, "Sensorless vector and speed control of brushless motor drives," *IEEE Trans. Ind. Electron.*, vol. 41, no. 1, pp. 91–96, Feb. 1994.

[3] G. Yang, R. Tomioka, M. Nakano, and T. H. Chin, "Position and speed sensorless control of brushless DC motor based on an adaptive observer," *IEEJ Trans. Ind. Appl.*, vol. 113, no. 5, pp. 579–586, May 1993.

[4] N. Matsui, "Sensorless PM brushless DC motor drives," *IEEE Trans. Ind. Electron.*, vol. 43, no. 2, pp. 300–308, Apr. 1996.

[5] G. D. Andreescu, "Position and speed sensorless control of PMSM drives based on adaptive observer," in *Proc. EPE*, Lausanne, Switzerland, Sep. 1999. [CD-ROM].

[6] M. Rashed, P. MacConnell, A. Stronach, and P. Acarnley, "Sensorless indirect rotor field orientation speed control of permanent magnet synchronous motor using adaptive rotor flux estimator," in *Proc. IEEE CDC-ECC*, Seville, Spain, Dec. 2005, pp. 647–652.

[7] A. Piippo and J. Luomi, "Adaptive observer combined with HF signal injection for sensorless control of PMSM drives," in *Proc. IEEE IEMDC*, San Antonio, TX, May 2005, pp. 674–681.

[8] S. Koonlaboon and S. Sangwongwanich, "Sensorless control of interior permanent-magnet synchronous motors based on a fictitious permanent-magnet flux model," in *Conf. Rec. IEEE IAS Annu. Meeting*, Hong Kong, Oct. 2005, vol. 1, pp. 311–318.

[9] S. Shinnaka, "New "D-State-Observer"-based vector control for sensorless drive of permanent-magnet synchronous motors," *IEEE Trans. Ind. Appl.*, vol. 41, no. 3, pp. 825–833, May/Jun. 2005.

[10] Z. Chen, M. Tomita, S. Doki, and S. Okuma, "An extended electromotive force model for sensorless control of interior permanent-magnet synchronous motors," *IEEE Trans. Ind. Electron.*, vol. 50, no. 2, pp. 288–295, Apr. 2003.

[11] M. Hinkkanen, "Analysis and design of full-order flux observers for sensorless induction motors," *IEEE Trans. Ind. Electron.*, vol. 51, no. 5, pp. 1033–1040, Oct. 2004.

[12] T. Jahns, G. Kliman, and T. Neumann, "Interior permanent-magnet synchronous motors for adjustable-speed drives," *IEEE Trans. Ind. Appl.*, vol. IA-22, no. 4, pp. 738–747, Jul./Aug. 1986.

[13] O. Wallmark and L. Harnefors, "Sensorless control of salient PMSM drives in the transition region," *IEEE Trans. Ind. Electron.*, vol. 53, no. 4, pp. 1179–1187, Jun. 2006.

[14] A. Piippo, M. Hinkkanen, and J. Luomi, "Sensorless control of PMSM drives using a combination of voltage model and HF signal injection," in *Conf. Rec. IEEE IAS Annu. Meeting*, Seattle, WA, Oct. 2004, vol. 2, pp. 964–970.

[15] J. K. Pedersen, F. Blaabjerg, J. W. Jensen, and P. Thogersen, "An ideal PWM-VSI inverter with feedforward and feedback compensation," in *Proc. EPE*, Brighton, U.K., Sep. 1993, vol. 5, pp. 501–507.

Antti Piippo (S'06) received the M.Sc.(Eng.) degree from Helsinki University of Technology (TKK), Espoo, Finland, in 2003.

Since 2003, he has been with the Power Electronics Laboratory, TKK. He is a Research Scientist in the Department of Electrical and Communications Engineering, TKK. His main research interest is the control of electrical drives.

Marko Hinkkanen (M'06) received the M.Sc.(Eng.) and D.Sc.(Tech.) degrees from Helsinki University of Technology (TKK), Espoo, Finland, in 2000 and 2004, respectively.

Since 2000, he has been with the Power Electronics Laboratory, TKK. He is currently an Acting Professor in the Department of Electrical and Communications Engineering, TKK. His research interests are in the areas of electric drives and electric machines.

Jorma Luomi (M'92) received the M.Sc.(Eng.) and D.Sc.(Tech.) degrees from Helsinki University of Technology (TKK), Espoo, Finland, in 1977 and 1984, respectively.

In 1980, he joined TKK, and from 1991 to 1998, he was a Professor at Chalmers University of Technology, Göteborg, Sweden. He is a Professor in the Department of Electrical and Communications Engineering, TKK. His research interests are in the areas of electric drives, electric machines, and numerical analysis of electromagnetic fields.